Variations in Microanatomy of the Human Cochlea

Ersin Avci,[1]* Tim Nauwelaers,[2] Thomas Lenarz,[1] Volkmar Hamacher,[2] and Andrej Kral[1]

[1]Cluster of Excellence Hearing4all, Institute of AudioNeuroTechnology and Department of Experimental Otology, Ear, Nose, and Throat Clinics, Hannover Medical University, Hannover 30625, Germany
[2]Advanced Bionics, European Research Center, Hannover 30625, Germany

ABSTRACT

The human cochlea shows considerable interindividual variability in size and morphology. In order to develop atraumatic cochlear implant (CI) electrodes, high-precision details of the variability of human anatomy are required. Sixteen human temporal bones were cut around the cochlea in blocks of approximately 3.5 × 3.5 cm. The bones were scanned by using a Skyscan 1173 micro-computed tomography (μCT) device. Mimics software (Materialise, Leuven, Belgium) was used to segment out the scala tympani (ST) from the μCT images. A three-dimensional surface model of the segmented area was generated for each cochlea. Cross-sectional images were taken and analyzed by custom-designed software in MATLAB. Comparison of different STs showed large variability in cross-sectional diameter (CSD), vertical trajectory, and height of the ST. Relative standard deviations of the CSD were between 9 and 15%. Heights measured at the center of the ST exceeded those in the modiolar and lateral regions of the scala. At the lateral region, the height decreased significantly at the beginning of the second turn. In the vertical trajectory, critical anatomic features were observed, such as dips, vertical jumps, and peaks. Rosenthal's canal (RC) extended to between 560 and 650°. We found a correlation between the length of the RC and that of the ST. The ST was segmented and the internal dimensions measured by using μCT. We observed large dimensional variability between different STs. These differences could have considerable implications for approaches to the design of CI arrays, especially in terms of their ability to preserve residual hearing during insertion of the electrode array. J. Comp. Neurol. 522:3245–3261, 2014.

INDEXING TERMS: cochlear implant; scala tympani; μCT; hearing preservation; individualized therapy

Subjects suffering from sensorineural deafness have been able to regain partial hearing and speech understanding by using cochlear implants (CIs) (Kral and O'Donoghue, 2010; Lenarz, 1999; Turner et al., 2004). CIs consist of an electrode array placed in the scala tympani (ST), under the basilar membrane and the osseous spiral lamina. It carries up to 22 stimulation contacts that deliver the current to the surviving auditory nerve fibers, bypassing the nonfunctional organ of Corti. The placement of the electrodes close to the auditory nerve fibers is of crucial importance for effective electrical stimulation (Holden et al., 2013; Min et al., 2013; Rebscher et al., 2008). The implantation procedure itself may result in damage to the cochlear structures (Helbig et al., 2011; Kha and Chen, 2012; Nadol et al., 2001; Richter et al., 2001; Tykocinski et al., 2001; Wardrop et al., 2005a). Such damage can in some cases lead to loss of spiral ganglion cells (Adunka and Kiefer, 2006; Leake et al., 1999; Roland and Wright, 2006; Simmons, 1967; Staecker et al., 1998), and therefore may negatively interfere with the outcome of cochlear implantation.

More recently, patients with significant residual hearing have been shown to benefit from a combination of electrical and acoustic stimulation (Cullen et al., 2004; Lenarz, 1998; Von Illberg et al., 1999). In these subjects, the implantation procedure has to be as atraumatic as possible, because any damage may affect the

Grant sponsor: Advanced Bionics; Grant sponsor: the German Research Foundation (DFG; Cluster of Excellence Hearing4all).

*CORRESPONDENCE TO: Ersin Avci, Cluster of Excellence Hearing4all, Institute of AudioNeuroTechnology and Department of Experimental Otology, ENT Clinics, Hannover Medical School, Hannover 30625, Germany. E-mail: Avci.Ersin@mh-hannover.de.

Received January 24, 2014; Revised March 21, 2014;
Accepted March 21, 2014.
DOI 10.1002/cne.23594
Published online March 26, 2014 in Wiley Online Library (wileyonlinelibrary.com)

function of the organ of Corti. However, CI electrodes need to be long enough to cover and stimulate a wide frequency range in the cochlea, and have to be positioned as close to the nerve fibers as possible. All of this increases the probability of cochlear damage. Preventing direct damage to soft tissues and osseous structures is an important factor for combined electrical and acoustic stimulation (EAS) (Gantz and Turner, 2003; Lenarz, 2009; Von Illberg et al., 1999). Detailed knowledge of the microanatomy is of crucial importance in preventing such implantation damage.

The human cochlea shows considerable interindividual variability in size and morphology (Biedron et al., 2010; Erixon et al., 2008; Escude et al., 2006; Hardy, 1938; Rask-Andersen et al., 2011; Shin et al., 2013; Verbist et al., 2009; Wysocki, 1999; Zrunek and Lischka, 1981). Even so, today CIs tend to have dimensions designed for one cochlear size only. Because of interindividual variations in anatomy and the goal of residual hearing preservation, a prosthesis needs to be tailored to the individual patient. To allow appropriate selection of a prosthesis for a given patient, detailed quantified information on the individual variations of the human cochlea is required.

In the past, evaluation of cochlear anatomy has been performed by means of clinical computed tomography (CT), plastic casts, or histological examinations (Biedron et al., 2010; Escude et al., 2006; Rask-Andersen et al., 2011). The disadvantage of histological examination is that the information is limited to midmodiolar sections. When three-dimensional (3D) reconstructions were attempted, they generally suffered from degraded spatial resolution (Biedron et al., 2010). Furthermore, the demineralization, fixation, and staining methods did not allow artifact-free measurements of the fragile inner structures of the cochlea, particularly in plastic casts that rendered them (in part) not visually accessible. Misalignment of the cochlear axis with the cutting plane may have influenced the outcomes, and in cases of 3D reconstruction the alignment of the sections was often not free of artifacts. CT is the only method that delivers noninvasive images of the cochlear geometry, but reconstruction of the sliced CT scans reduces image resolution and creates artifacts (e.g., partial volume effect). Cone beam CT avoids some of the disadvantages of multislice CT, but is still insufficient to provide the internal dimensions of the cochlea.

To measure the internal dimensions and assess the variability of different cochleae with high precision, microcomputed tomography (μCT) was used in the present study. μCT can acquire images in pixel size of few μm. This imaging technique, combined with a modified preparation technique, allowed high-resolution visualization of the cochlear structures in all three dimensions. We were able to successfully quantify the internal dimensions and morphology of the cochlea with a precision exceeding that of previous investigations. The present study identified the three anatomic positions in the cochlea that are the most likely site of implantation damage. Finally, and for the first time, the present study analytically describes the relation between the anatomic dimensions and the location of the implant within the scala, with particular emphasis on the insertion depth of the implant.

MATERIALS AND METHODS

Preparation of human cochleae

For this study, 16 fresh-frozen human temporal bones without any evidence of malformation were analyzed. Ten left and six right temporal bones were used. The fresh-frozen bones were slowly thawed at room temperature, and were subsequently cut around the cochlea in blocks of approximately 3.5 × 3.5 cm, containing the outer, middle, and inner ear. This procedure has been shown to preserve the cochlea well, including its micromechanical properties (Ravicz et al., 2000; Rosowski et al., 1990). To gain access to the inner ear, a standard mastoidectomy and posterior tympanotomy were performed. This approach allowed direct access to the inner ear. The cochlear fluid (perilymph) and the fine structures in the cochlea have a similar X-ray attenuation coefficient, which reduces the resulting image contrast. To visualize the fine structures in the cochlea, the round window (RW) membrane was opened and a small opening at the oval window was drilled. By using a suction tube and the two openings (round and oval windows), the cochlear fluid was gently removed at the RW. This intervention allowed a substantial increase in the image contrast between the soft tissue (basilar membrane, spiral ligament, endosteum) and the scalae. Subsequently, the cochlea was wrapped with formaldehyde-immersed cotton tissue for fixation. The subsequent μCTs were used to assess the quality of the storage and preparation technique. In all cochleae used, no damage of the microanatomy was observed attributable to preparation and fixation. Figure 1 shows the difference between image quality in fluid-filled (Fig. 1A) and air-filled (Fig. 1B) scalae.

Scanning, segmentation and reconstruction

The temporal bones were scanned by using a high-energy μCT device (Skyscan 1173, Brucker, Belgium). It included a 130-kV microfocus X-ray source within which the specimen was rotated 360° between the X-ray source and the camera. Rotation steps between 0.2 and 0.3° were used. At each angle, an X-ray exposure was recorded on the distortion-free flat-panel sensor (resolution: 2,240 × 2,240 pixels, 5 Mp). To further

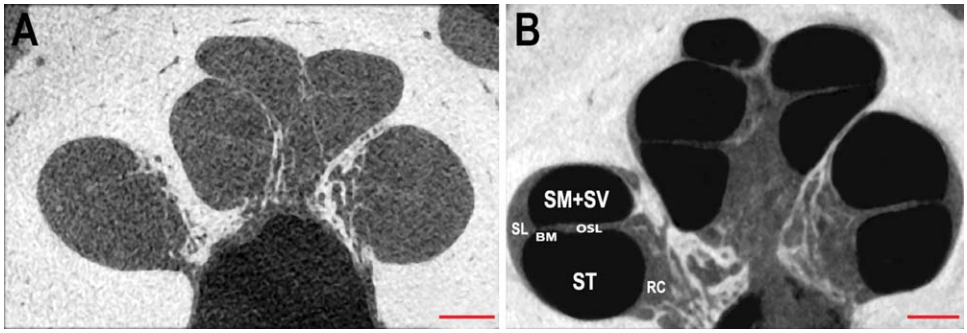

Figure 1. **A,B**: The μCT image of a fluid-filled (A) and air-filled (B) human cochlea. Resolution: 10 μm. The fluid-filled image is noisier due to the minimal difference of the linear attenuation coefficient of the perilymph and the soft tissue (A). In the air-filled image, the fine structures (ST, scala tympani; SV, scala vestibuli; RC, Rosenthal's canal; SL, spiral ligament; BM, basilar membrane, and OSL, osseous spiral lamina) are clearly visible. The extremely thin Reissner's membrane, which separates the scala media (SM) and SV, is not visible (B). Scale bar = 1 mm in A,B.

increase the contrast, a 0.25-mm brass filter was used. To reduce the noise, long integration times were allowed, resulting in scan times of approximately 3 to 5 hours for each specimen; images with isotropic voxel size varying from 8 to 17 μm were achieved in most cases; in five cases it was 36 μm.

The (TIFF) images acquired were reconstructed by using NRecon reconstruction software (Skyscan). The reconstructed images were reoriented: the central axis (through the center of the modiolus and the helicotrema) of the cochlea was moved to the vertical direction, and then entire cochleae were reoriented based on the cochlear coordination system (Verbist et al., 2010) so that individual cochleae could be directly matched and compared. Then Mimics software (version 14.0, Materialise, Leuven, Belgium) was used to segment out the ST, Rosenthal's canal, the RW, and the central axis of the cochlea from each of the image data sets. The precise interpolation function of the MIMICS software allowed us to semiautomatically segment between the image slices. For every 10th image slice, the region of interest was marked and subsequent images were interpolated, giving the most exact, safe, and fast segmentation. To obtain the complete geometry of the ST, segmentation was performed in both the transversal and coronal views.

Registration, measurement, and statistical analysis

All the right cochleae were mirrored to left cochleae. To compare dimensions of multiple cochleae, the centers of the RW were merged, and the z-axes (connecting the center of the modiolus [central axis] and the helicotrema) were placed in parallel, as were the axes running from the center of the RW toward the central axis (see Fig. 6B). To measure cochlear dimensions, the standard cochlear coordinate system was used (Verbist et al., 2010). The starting point for measuring the cochlear length was the inferior edge of the RW. A line connecting the center of the long diameter of the RW and the central axis of the center of the modiolus was the reference line for angle measurements (0° reference angle).

To measure the internal dimensions of the ST, cross-sectional images were used. To obtain these, slices were taken every 0.1 mm orthogonal to the centerline and along the lateral wall of the ST for two cochlear turns. The slices were subsequently analyzed by custom-designed software programmed in MATLAB (RRID:nlx_153890; MathWorks, Natick, MA) (Fig. 2). This software calculated the cross-sectional diameter (CSD), the area of the ST, the height profile, and the vertical trajectory of the 16 scalae. Calculation of the CSD was performed by distance transformation, where the distance between each pixel (inside the cross-sectional contour) and the nearest non-zero pixel (boundary of the contour) were calculated. The point that lies inside the contour and is furthest from the closest edge defines the center of the largest circle.

To calculate the angle–distance relation, the distance along the ST was obtained every 15° starting from the anterior/inferior edge of the RW up to the 720° position. All data were collected and analyzed by using MATLAB (RRID:nlx_153890), and the curve-fitting toolbox was used to calculate best fitted functions.

Statistical analysis involved calculation of the average, standard deviation, and relative standard deviation for each measurement. Statistical testing was performed by using one-way analysis of variance (ANOVA) and regression analysis. Measurement errors introduced during registration and segmentation of the scalae were between 30 and 50 μm.

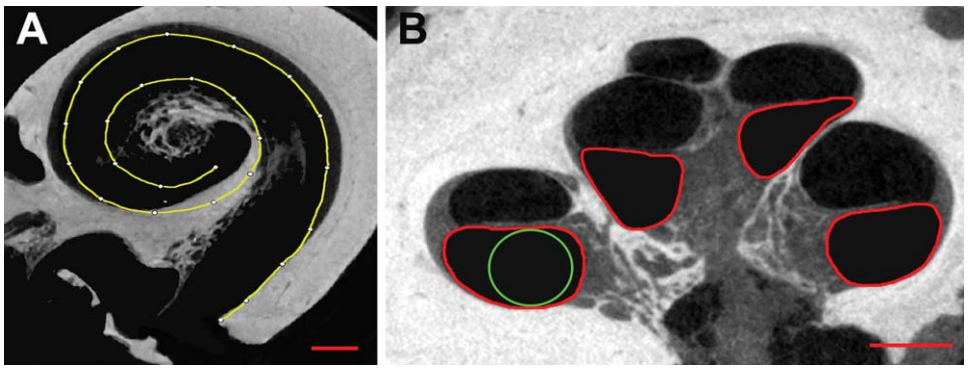

Figure 2. **A**: Cross sections taken perpendicular to the yellow line along the scala tympani, every 0.1 mm. **B:** The red lines show the contour of the segmented area, and the green line shows the largest circle for that segment. The images were exported to MATLAB and analyzed further. Scale bar = 1 mm.

RESULTS

Analyses of the μCT images confirmed the absence of any mechanical trauma. Thus, the preparation method and the removal of cochlear fluids proved a reliable method for allowing assessment of the cochlear anatomy. However, complete removal of the fluid could not be achieved in all cases, because suction pressure had to be limited so as not to destroy the fragile structure of the cochlea. Therefore, the most apical half-turn of the scalae could not be assessed with confidence in all cochleae. Consequently, some of the present scaleae measurements could only be used to analyze the basal two turns. This is also the relevant portion of the cochlea where the majority of CIs are located.

Characteristic features of the cochleae were easily discernible in the midmodiolar sections (Figs. 1–3); however, significant interindividual variability in morphology was observed. The scalae had a regular oval shape in the basal turn. In the middle turn, the shape was more vertical, particularly for the ST at the place where the middle turn spatially approached the basal turn (also discernible in Figs. 1–3).

Basic measurements

Height, width, length, cochlear turn, and round window diameter

Basic measurements of the cochlear dimensions included cochlear axis height, width of the cochlear base, and length of the cochlear base (Fig. 3). All results are included in Table 1 and show variability of the basic cochlear parameters ranging from 12 to 19% of the maximum value. There was a significant positive correlation between length of the cochlear base (LCB) and width of the cochlear base (WCB) ($R^2 = 0.71$, $P < 0.01$; Fig. 4). Interestingly, not only the length but also the number of cochlear turns was variable, the mean being 2.64 ± 0.17 ($949 \pm 62°$), ranging from 2.39 to 2.84 (859–1,024°). This demonstrates that the individual cochleae are not simply scaled versions of the same blueprint but have truly different morphologies.

To investigate whether cochleae with a smaller base are of greater height, correlations between base measurements and cochlear height were assessed. The correlation, although partially significant, was rather weak (LCB: $R^2 = 0.33$, $P = 0.02$; WCB: $R^2 = 0.18$, $P < 0.11$; $\sqrt{(LCB^2 + WCB^2)}$: $R^2 = 0.29$, $P < 0.03$). This calculation

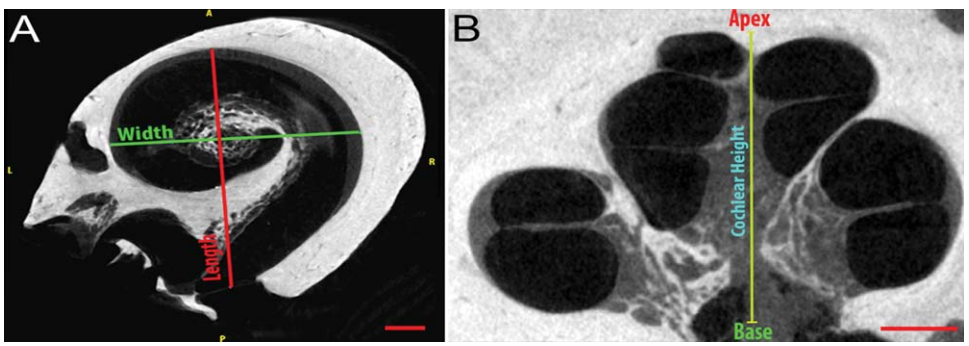

Figure 3. **A,B**: Measurement of the width and length of the cochlear base (A) and the cochlear axis height (B).

TABLE 1.

Basic Cochlear Measurements as Determined From the μCT Measurements

TB	Height (mm)	Length (mm)	Width (mm)	CT	RW (mm)	AP (degree)
1	4.5	9.1	7.1	2.78	1.34	615
2	4.1	8.5	6.7	2.39	1.03	555
3	4.7	9.6	7.6	2.42	1.31	585
4	4.2	9.1	6.9	2.46	1.31	585
5	4.6	9.8	7.3	2.78	1.18	555
6	4.0	8.9	6.8	2.70	1.37	555
7	4.6	9.4	7.2	2.79	1.12	600
8	4.5	8.9	6.9	2.78	1.18	600
9	4.4	9.3	7.1	2.48	1.28	540
10	3.9	9.2	7.0	2.59	1.19	510
11	4.3	9.9	7.4	2.45	1.22	525
12	4.8	10.1	7.4	2.83	1.30	540
13	3.9	8.8	6.8	2.43	1.16	585
14	4.6	9.0	7.0	2.66	1.24	570
15	4.7	9.1	6.5	2.79	1.34	555
16	4.1	8.8	6.9	2.84	1.00	570
Mean	4.4	9.2	7.0	2.64	1.22	565
SD	0.3	0.4	0.3	0.17	0.11	29

Abbreviations: TB, temporal bone number; CT, number of cochlear turns; RW, round window maximum circular diameter; AP, angular position; SD, standard deviation.

demonstrates that cochleae with a broader base tended to be of greater height, but additional factors need to be taken into account that influence this relation.

The length of the basal two turns along the lateral wall of the ST ranged from 30.1 to 35 mm (32.1 mm ± 1.5 mm). For the central position, the mean length was 23.6 ± 1.1 mm (range: 21.9–26.3 mm).

The size of the RW was quantified by the diameter of its largest fitted circle (1.22 ± 0.11 mm, ranging from 1.00 to 1.34 mm). The maximum RW height (short diameter) was 1.50 mm, whereas the maximum RW width (long diameter) was 1.72 mm.

Rosenthal's canal

A positive correlation was found between the length of Rosenthal's canal and the length along the center of the ST ($R^2 = 0.83$, $P < 0.01$, Fig. 5). Rosenthal's canal thus extends proportionally to the length of the ST. The ratio between the spiral ganglion length and the lateral wall length was similar in different cochleae (mean of 0.9 ± 0.2). The mean angular position of the end of Rosenthal's canal was 565 ± 29° from the anterior/inferior edge of the RW, ranging from 510 to 615° (Table 1). This implies that, in longer cochleae, the spiral ganglion cells are also distributed over a longer cochlear distance. In other words, it is not the spread of the primary afferents that compensates for the longer dimension of the scalae in large cochleae, but rather the length of Rosenthal's canal itself.

Advanced measurement of the scala tympani

The 3D reconstructions of the ST demonstrate that there is considerable variability in size and shape that can even be observed in the macroanatomy of the cochlea (Fig. 6). The differences are appreciable—in the mm range—and some of them can potentially be detected by using clinical CT imaging as well.

Height measurement of the scala tympani

The height of the ST was measured at three locations: the lateral height at 0.2 mm from the lateral wall, the modiolar height at 0.2 mm from the modiolar wall, and the center height at the middle of the most modiolar and most lateral location of the scala. The mean height ± 1 standard deviation was then plotted against

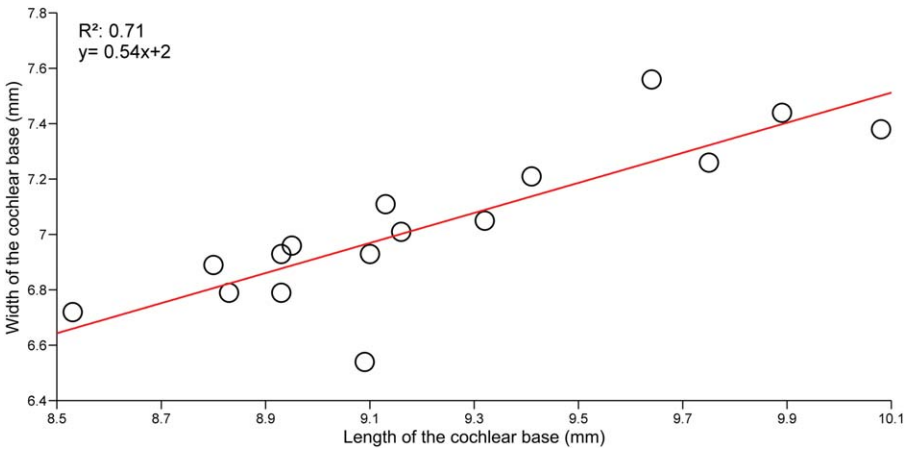

Figure 4. Correlation between length of the cochlear base (largest distance from the round window, through the central axis, to the lateral wall) and width of the cochlear base (perpendicular distance at the central axis); red line indicates the linear fit.

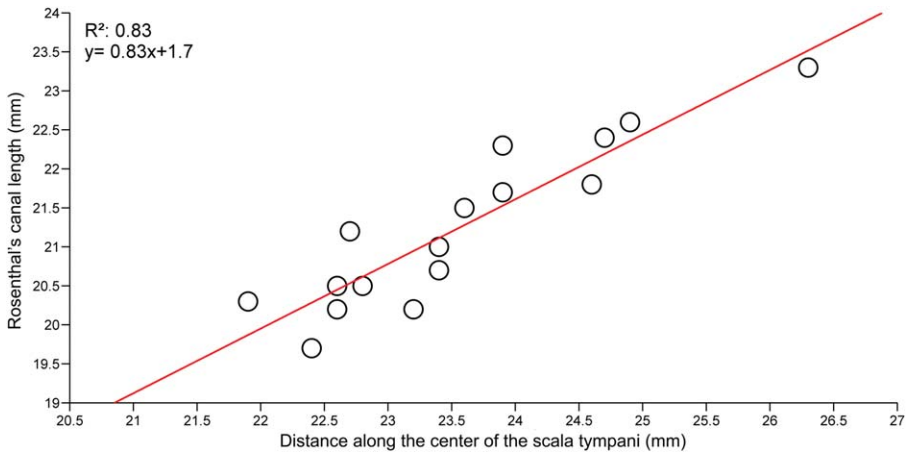

Figure 5. Correlation between Rosenthal's canal length and the length along the scala tympani (ST) for the first two turns; red line indicates the linear fit. The length of the ST is measured along its center.

the angular distance from the anterior/inferior edge of the RW (Fig. 7).

The height was largest at the center of the ST, whereas the modiolar and lateral height were significantly lower ($P < 0.01$, ANOVA; Fig. 7). The height at the lateral wall decreased significantly after 450°, whereas the modiolar height remained more or less similar along the cochlear length. The mean height at the modiolar wall increased within the first 30 to 40° (3–4 mm) and decreased gently until the 180° position was reached (~12.5 mm), remaining constant from that point on until the end of the second cochlear turn. From the RW to the end of the second turn, the mean modiolar height decreased from 0.82 ± 0.09 mm to 0.72 ± 0.11 mm. The mean height at the lateral position increased within the first 20° (1.5 mm). From 20 to 60° (1.5–5 mm), the mean height decreased substantially and remained constant until 450°. Beyond 450°, the height decreased considerably until the end of the second cochlear turn. From the RW to the end of the second turn, the mean lateral height fell from 0.86 ± 0.23 mm to 0.35 ± 0.09 mm. The mean height at the central location decreased within the first 30° (3 mm) and continued to fall slowly until the 130° position

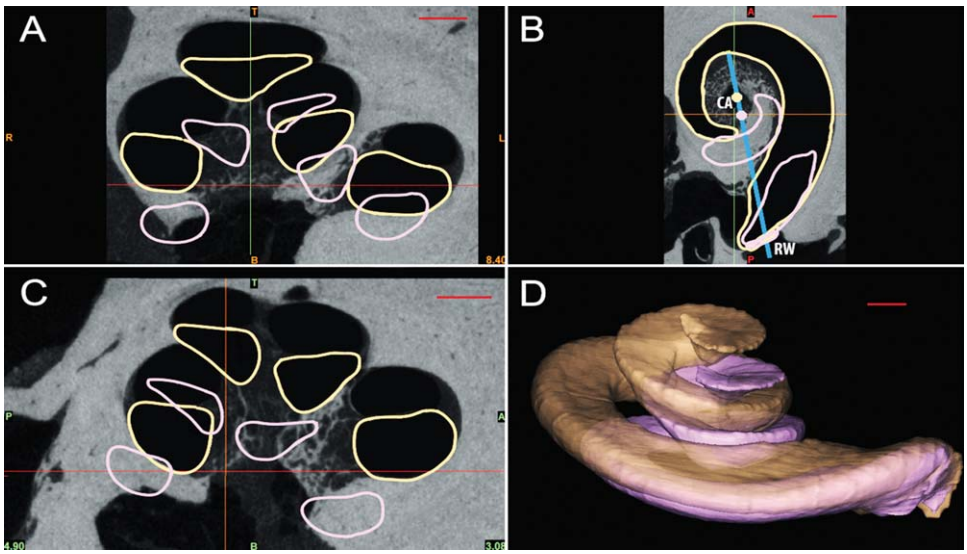

Figure 6. **A–C**: Cross-sectional view of two cochleae in coronal (A), sagittal (C), and cochlear views (B). **D:** Three-dimensional surface reconstruction of the scala tympani with the largest (beige, TB11), and smallest (pink, TB06) cross-sectional diameter observed in 16 temporal bones (see Fig. 8). The large dimensional variability between the largest and smallest scala tympani is clearly visible. CA, cochlear axis; RW, round window. Scale bar = 1 mm.

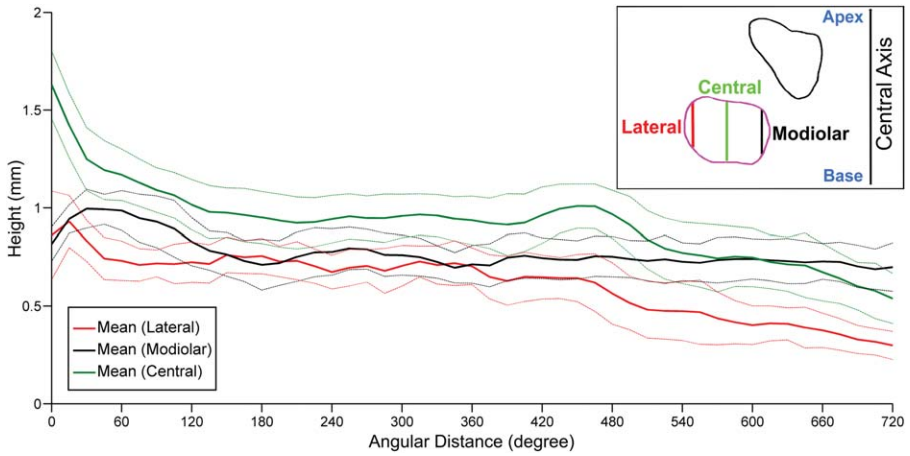

Figure 7. Mean height of the scala tympani (solid lines) with ± 1 standard deviation (dotted lines) as a function of angular distance. The largest height is at the center (green) of the scala tympani, where the modiolar height (black) remained nearly constant, and the lateral height (red) decreased markedly after 450°. At the end of the second turn (600–720°), the mean modiolar height exceeds the mean central height.

was reached (10 mm). From 130 to 380° (10–22 mm), the mean height remained constant. Following a slight increase, the height decreased substantially until the investigated cochlear partition was reached. From the RW to the end of the second turn, the mean central height fell from 1.63 ± 0.18 mm to 0.65 ± 0.14 mm.

Taking everything into account, this means that in the apical direction the ST narrows mainly at the antimodiolar position (as can be observed also in midmodiolar sections in Figs. 1–3), the consequence being that a laterally positioned cochlear electrode array tends to be pushed either against the basilar membrane or in the modiolar direction (in more flexible electrode arrays).

Cross-sectional diameter and sectional area of the scala tympani

The cross-sectional diameter (CSD) was evaluated by fitting the largest possible circle inside the ST boundaries. This technique allows assessment of the maximum dimensions of a round electrode array that fits into the human cochlea, whereas the sectional area illustrates the maximum volume in the corresponding region. As mentioned above, the main change in the internal dimensions of the ST in the apical direction is found in the antimodiolar portion, but this also affects the size of the electrode array that fits into the ST at a given angular position.

The largest circle was computed by using distance transformation, whereby the center of the circle is the point furthest from the closest edge. The individual and the average CSD were plotted against the angular distance from the anterior/inferior edge of the RW. The software calculated the sectional area (SA) as the sum of all pixels inside the contour.

The average cross-sectional diameter (aCSD) reached a maximum within the first 20° (~1 mm laterally from RW; Fig. 8). From there, the aCSD decreased until the 180° position (~11 mm laterally from RW). It decreased by about 350 μm from 20 to 180°, and remained constant until the 400° position (~21 mm) was reached. After a slight increase between 400 and 450° (~21–23 mm), the aCSD decreased until the end of the second turn. The aCSD decreased from the base to the end of the second turn by approximately 300 μm. The variability of the CSD between each of the 16 scalae was 9–15%. Furthermore, the overall pattern and the position of the minima and maxima in CSD showed interindividual variation (Fig. 8).

The average sectional area (aSA) followed a similar pattern as the aCSD. Within the first 20°, the aSA reached a maximum of 2.3 mm^2, and decreased until the end of the second cochlear turn to 0.6 mm^2 (Fig. 9). The variability of the SA between each of the scalae was higher compared with the CSD (14–24 %). TB06 and TB11 represent the ST with smallest and largest aCSD and aSA.

To quantify the optimal position of the electrode array giving the smallest probability of damaging the basilar membrane, we also calculated the relative position of the center of the largest circle in the horizontal plane of the cross section (Fig. 10). The location of the circle was relatively constant and was located at the center or center/modiolar region of the scala. This illustrates again that the largest space is located at the central region of the ST and that, at this position, the likelihood of contact with the cochlear structure is lowest.

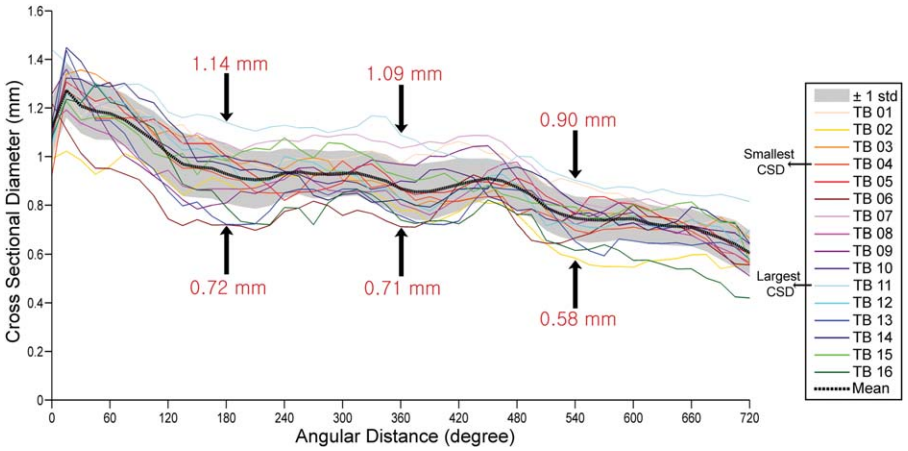

Figure 8. The average cross-sectional diameter (aCSD; black) and individual cross-sectional diameter (CSD; colored) as a function of the angular distance based on the largest circle that could fit into the cochlear scala for each segment. The aCSD increased within the first 20°, and decreased until the end of the second cochlear turn.

Angle–distance relation

Two different measures of cochlear length have been used in the literature: angular and length measures. In principle, the cochlea can be larger (or smaller) in length without changing the angular length (proportional increase in size in all directions), or it can become larger by increasing both the length and the angular measure (true lengthening of the cochlea). To investigate this variability, we directly compared the angular and distance lengths (Fig. 11).

Due to the straight basal segment of the first cochlear turn, the angular distance changed slowly until the 45° position was reached. With increasing angular distance, the difference between the central and lateral distance increased. The first cochlear turn (360°) covered 21.0 ± 0.99 mm along the lateral wall, and 16.6 ± 0.76 mm along the center of the ST. An electrode whose position extended up to 21 mm along the lateral wall would cover 315–400°, whereas an electrode whose position extended up to 28 mm along the lateral wall would cover 510–645°. The overall length of the first two turns (when measured as angular distance) covers 31.9 ± 1.5 mm at the lateral wall and 23.5 ± 1.0 mm at the center of the scala. Consequently, the location within the ST is a critical parameter for determining the optimal length of the electrode array. Based on the data, an exponential function was fitted to determine the distance along the ST:

$$y(x) = Ae^{-bx} + C \quad (1)$$

where x is the angular distance of the ST, y is the distance along the ST, and parameters A, C, and b were determined

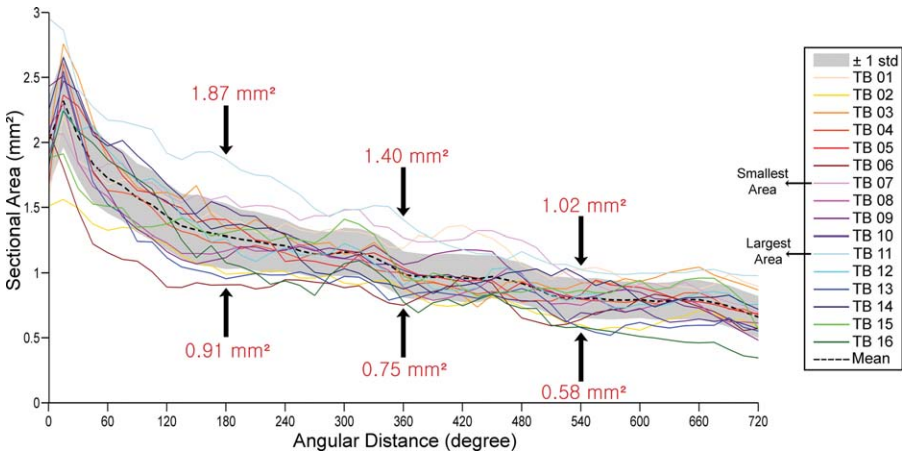

Figure 9. The average sectional area (aSA; black-dotted) and individual sectional area (SA; colored) as a function of the angular distance. The aSA increased within the first 20°, and subsequently continuously decreased until the end of the second cochlear turn. RW, round window.

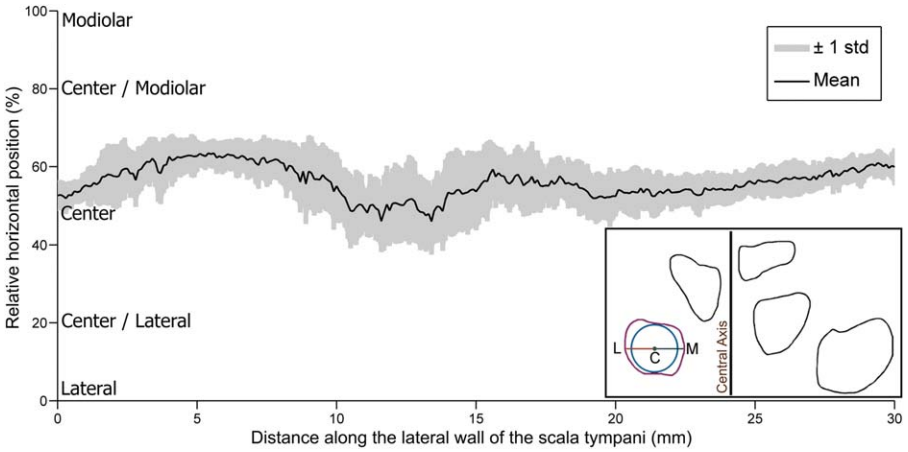

Figure 10. The average horizontal position of the largest circle of the scala tympani (ST). Horizontal distance from the center of the circle (C) to the lateral edge (L) was used to calculate the relative position of the circle. The largest circle was mainly located at the center-modiolar region of the ST.

by a fitting procedure (for the lateral length: $A = -42.230$, $C = 42.892$, $b = 1.8384 \times 10^{-3}$, $R^2 = 0.999$; for the central length: $A = -27.478$, $C = 28.451$, $b = 2.360 \times 10^{-3}$, $R^2 = 0.999$) .

Furthermore, taking into account the interindividual variability in cochlear implantation requires an estimate of the cochlear length using measures that can be obtained from conventional tomography and clinical CT. To calculate the required insertion depth of a CI within the ST from a desired angular distance determined in preoperative imaging, the following equation can be used:

$$D_{\mathrm{id}} = \left((Ae^{-bx}) + C\right) * \left[1 + \left(\frac{LCB - LCB_{\mathrm{Mean}}}{LCB_{\mathrm{Mean}}}\right)\right] \quad (2)$$

where D_{id} is the insertion depth along the scala (D_{CL}: central; D_{LW}: lateral); x is the desired angular distance; LCB is the length of the cochlear base; LCB_{Mean} is 9.2 mm (mean length of the cochlear base; see Table 1); and the parameters A, b, and C are chosen depending on which location of the implant is assumed, central or lateral).

Depending on which parameters A, b, and C are used for the equation, insertion depths for central or lateral locations of the implants can both be calculated. For example, the LCB measured is 8.8 mm, the desired angular distance is 360° from the RW, and the implant is assumed to be in the lateral position. The predicted insertion depth along the ST is then

$$D_{LW} = \left((-42.230 * e^{-0.0018384*360}) + 42.892\right) * \left[1 + \left(\frac{8.8 - 9.2}{9.2}\right)\right] = 20.2\ \mathrm{mm}$$

whereas the measured insertion depth along the lateral wall in this cochlea is 20.0 mm. The difference between prediction and reality is thus 0.2 mm, i.e., 0.99%.

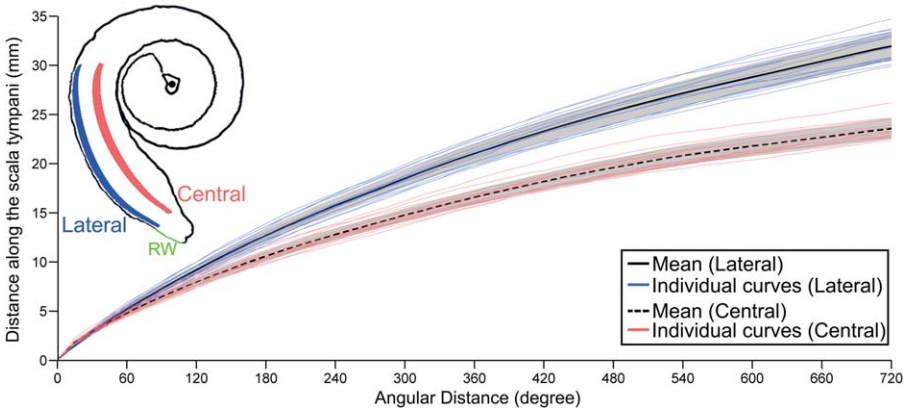

Figure 11. The average and the individual distance along the scala tympani (measured at the central and lateral position) as a function of the angular distance. The gray vertical lines indicate ± 1 standard deviation.

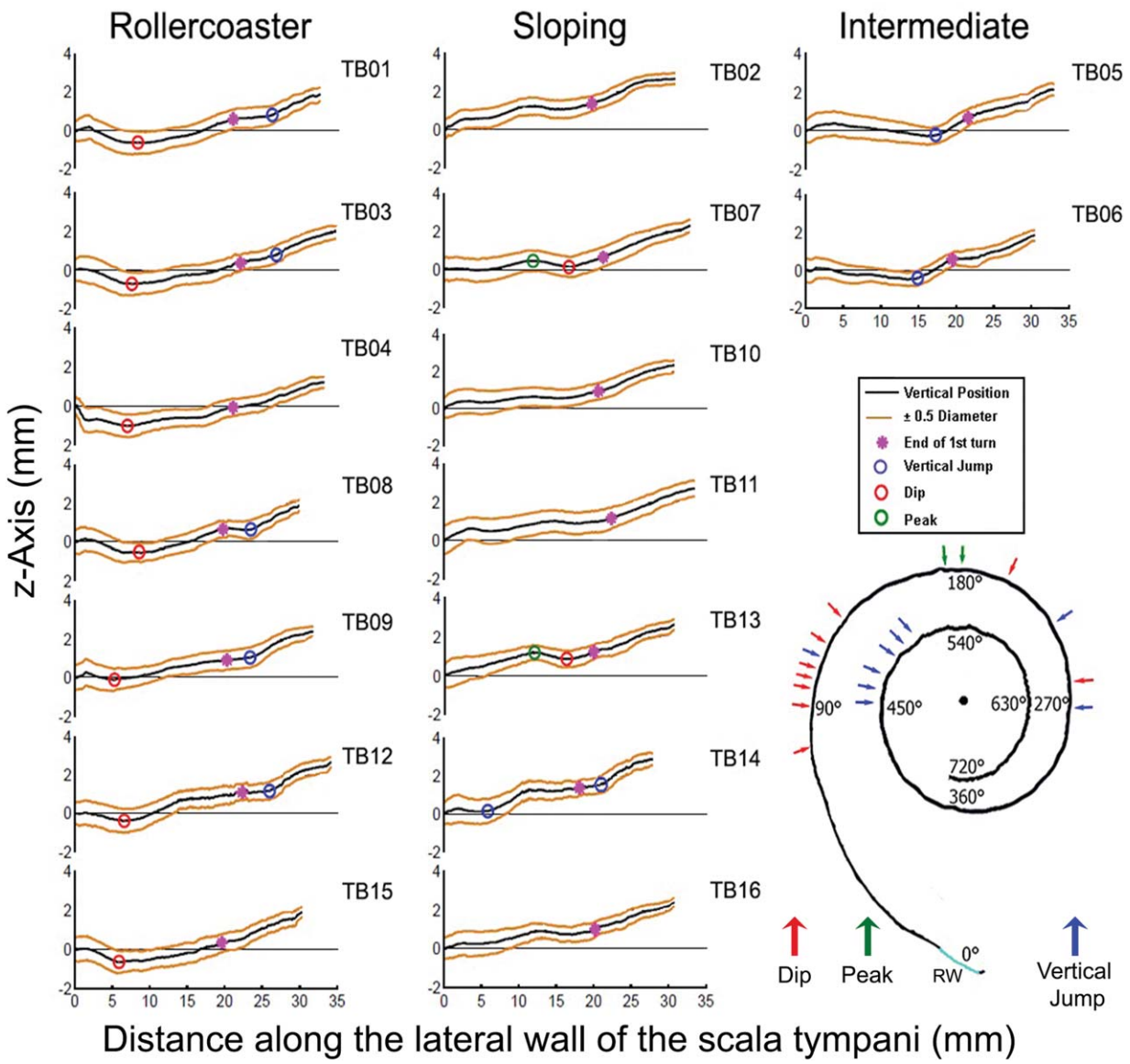

Figure 12. Vertical trajectory of different scalae tympani (ST). Relative position (relative to round window [RW]) of the largest circle's vertical coordinate (z-axis) is plotted (black line) against the distance along the ST (starting from the inferior edge of the RW). The orange lines mark the limits (i.e., the diameter) of the different ST. Bottom right: Schematic representation of a cochlea to visualize the angular position for each characteristic point in individual cochleae.

To further quantify the error of this analytical solution, the prediction based on the equation was compared with the actual lengths from all the 16 cochleae used for the 360° and 720° insertion angle. For the lateral wall position, the mean relative difference between actual and predicted values (prediction error) for 360° was 1.9 ± 1.4%; for 720° it was 2.7 ± 1.8%. For the central position and 360°, the prediction error was 2.2 ± 1.9%, and for 720° it was 2.3 ± 1.6%. In total, the prediction errors were larger for the lateral positions and the deep insertions. The cochleae with extreme values for the distance–angle relation (Fig. 11) gave the largest prediction errors. The maximal prediction error found was 5.4%. A prediction error of such low magnitude demonstrates that the analytical solution represents a very good estimate of possible implant insertion depths.

Vertical trajectory of the scala tympani

Another critical parameter with regard to cochlear implantation is the vertical profile of the ST, which is likely to influence the anatomic position of the implant and possible cochlear damage associated with the implantation. To assess this, the ST was unrolled and

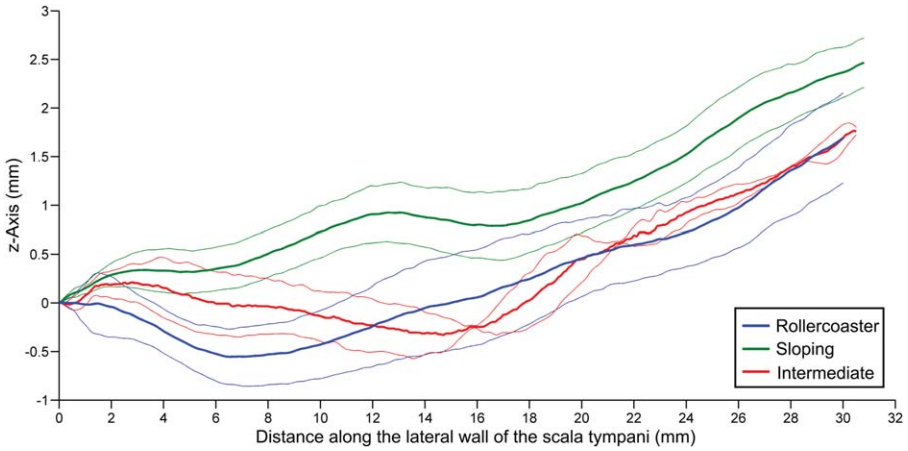

Figure 13. The mean vertical trajectory curve for each category. Critical anatomic features were found at individually different positions along the scala tympani (ST). Here, the rollercoaster category appears critical for cochlear implantation, as it can force the electrode array initially into the downward direction and subsequently into the upward direction. This may lead to damage to the basilar membrane and penetration into the scala vestibuli at the 180° position. The sloping category has a critical position at 12 mm from the round window (RW), where a distinct peak in the vertical direction may favor basilar membrane damage. The intermediate category would have a probability of damage highest at 20 mm from the RW.

the z-coordinates were compared by plotting the z-coordinates (vertical) of the largest circles (used to calculate the CSD) against the lateral wall distance of the ST (Fig. 12-13). All plots were normalized relative to the RW location and plotted in distance coordinates. The positions of critical changes in the z-axis were also assigned to angular coordinates (Fig. 12, inset).

Based on the vertical trajectory, three critical anatomic features were identified:

dip: a local minimum, if the downward slope was above 5° and the height difference above 0.3 mm (the assumed approximate radius of the implant carrier), followed by an increase in the vertical trajectory

peak: a local maximum, i.e., an increase followed by a decrease in the vertical trajectory, high difference of 0.3 mm

vertical jump: a sudden increase in the vertical trajectory, if the upward slope was larger than 10°.

The location for each of the points was also measured as a function of angular position relative to the RW and plotted on a schematic representation of the cochlea (Fig. 12, inset).

There was significant variability in the vertical trajectory between different STs. Due to the characteristic trajectories, the scaleae were classified into three categories. The scalae in the rollercoaster category all follow a downward trajectory from the RW, changing to upward course between 5 and 10 mm (75–120°), thus creating a dip in the vertical trajectory. The scalae in the sloping category all follow an upward trajectory from the RW without significant downward trends. Local peaks appeared only in this category (two of seven cochleae), and were located between 10 and 15 mm from the RW (around 180°). Between approximately 180 and 360° from the RW (15–20 mm), the profile remained temporarily flat in most cases. The scalae of the intermediate category have a local increase in the z-direction at the beginning, followed by a gradual decrease up to 15 mm from the RW. From this point on, the vertical position increased substantially until the end of the second turn. In seven cochleae a clear dip was observed between 5 and 8 mm, and in two between 15 and 20 mm from the RW. In six cochleae, vertical jumps were observed between 22 and 30 mm, and in three between 6 and 16 mm. Two scalae had peaks between 11 and 14 mm. Only four of the 16 cochleae investigated (25%) were devoid of any critical anatomic features (Fig. 12).

The most frequent occurrence of critical points was observed in the rollercoaster category, including the sequence of the descending–ascending course of the ST, combined with the vertical jump near the beginning of the second turn. Identifying this type of cochlear profile would be important in preventing cochlear damage. Use of particularly flexible CIs or implants with midscalar positioning of the electrode would decrease the probability of cochlear damage. Furthermore, the location of the cochleostomy and a controlled insertion angle might further reduce damage.

DISCUSSION

The present study is the first report providing statistical analysis of detailed microanatomic measures of human STs using μCT measurements. It was possible to investigate cochlear microanatomy following precise virtual alignment according to the cochlear coordinate system and virtual sectioning perpendicular to the ST at a given position.

This study identifies critical anatomic features where damage with CIs is likely to occur. Such features were found in the majority (75%) of the cochleae investigated. The study shows that the best atraumatic position of the implant would be a central one between the modiolar and the antimodiolar wall. We provide a detailed anatomic quantification of the ST that can be used as a reference for refined and individualized CI electrode arrays. Finally, the study makes an analytical tool available that allows assessment of the appropriate length of the electrode array in the individual patient from parameters obtained in conventional CTs. This approach may reduce the probability of cochlear trauma after implantation by proper selection of the electrode and the insertion depth.

The present study further confirms the high interindividual variability of the microanatomy of human cochlea. The large variability of the cochlear size opens questions with regard to its functional consequences. It remains to be investigated whether larger cochleae contain more hair cells and spiral ganglion cells, or, alternatively, whether these have a larger spacing. This might endow subjects with larger cochleae with a greater hearing range or higher hearing acuity (smaller, just noticeable difference in frequency). Such correlations have not yet been investigated.

Methodological issues

The techniques we used to prepare the cochlea and for μCT imaging enabled us to image the intracochlear structures with a resolution not available when using clinical CT or plastic casts. Owing to the high voxel resolution and enhanced contrast achieved, finding the internal boundaries for measurements led to small measurement errors (maximum segmentation error: ± 20 μm). Thin orthogonal reslices (100 μm) along the ST allowed a detailed study of the dimensional variability without loss of information. Measurements were taken within two cochlear turns because, in a few bones, the presence of residues at the apical turn led to a decrease in both the resolution and precision of measurements. The residue in the perilymphatic spaces of the cochlea could either be residual fluid or protein deposits. Nonetheless, as a rule, the CI electrode arrays and the spiral ganglion cell bodies typically do not extend beyond two turns.

The present study had the advantage of exact virtual alignment of the cochlea before measurements were taken. Slight inclination of the modiolar axis, for example, may lead to oblique cutting of the cochlea with over- or underestimation of cochlear dimensions. The method of 3D assessment and reconstruction presented here can therefore be considered much more precise than those of previous studies. Furthermore, the present fixation method is less susceptible to shrinkage.

However, the limitation of the study is that we could not relate the variability in morphology to data from the subject (gender, weight, height, etc.). Although it is likely that subjects with a large head size might have larger cochleae, we were not able to perform any quantification of such relations, owing to the anonymity of the bones' donors and to university policies regarding donation procedures. Previous studies indicate that females may have smaller cochleae than males (on average $\sim$1 mm length; Hardy, 1938; Miller, 2007). Finally, in the present study we mirrored six cochleae to so all the specimens could be compared. Previous studies demonstrated that the paired difference between the ears is small and nonsystematic in individual subjects (Hardy, 1938; Miller, 2007), and therefore the mirroring procedure does not impose any significant bias on the data.

A further limitation of the present technique is the lesser discernibility of soft tissue compared with histological studies (Postnov et al., 2006). Obviously, for this purpose histological methods are more appropriate. The complete length of the basilar membrane could not be measured due to difficulties in removing the cochlear fluid or protein deposits from the apex, and therefore this measure was not included in this study. Nonetheless, it was possible to perform assessments of the basilar membrane in the first two turns and the spiral ligament with confidence. Other soft tissue structures were not the focus of this study.

In several of the present measurements of the ST, instead of looking at the maximum or minimum dimensions, we fitted a circle into the ST and determined the diameter of the largest circle and its position. This approach is obviously focused on cochlear implantation and precludes a direct comparison with some of the measures used in previous studies.

Basic measurements

The estimated cochlear sizes based on preoperative CT scans of CI candidates were in accordance with our basic measurements obtained by using μCT. Our

cochlear axis height measurements were in agreement with previous reports (Dimopoulos and Muren, 1990; Erixon et al., 2008; Shin et al., 2013) that determined the mean cochlear axis height to be 3.9 mm with a range from 3.1 to 5.0 mm. The present count of cochlear turns is also in agreement with previous investigations (Erixon et al., 2008; Kawano et al., 1996; Shin et al., 2013; Skinner et al., 2002). Our mean LCB and mean WCB measurements were in accordance with Escude et al. (2006), and Erixon et al. (2008); the mean values from Dimopoulos and Muren (1990), and Martinez-Monedero et al. (2011) were slightly smaller. Escude et al. (2006) measured the parameters based on clinical CT images (mLCB: 9.23 ± 0.53 mm; mWCB: 6.99 ± 0.37 mm), whereas Erixon et al. (2008) measured parameters on plastic casts (mWCB: 6.8 mm, range: 5.6–8.2 mm). By using plastic casts, Dimopoulos and Muren (1990) determined the transverse diameter (measured in front of the RW across the central modiolar axis to the opposite side of the cochlea) with an mLCB of 8.58 ± 0.45 mm (range: 7.0–9.8 mm), whereas Martinez-Monedero et al. (2011) measured the dimensions from 3D models of CT images (mLCB: 8.62 ± 0.49 mm; mWCB: 6.55 ± 0.47 mm). These slightly smaller mean values in the previous studies may result from the measurement method (plastic casts and clinical CT images as opposed to μCT in the present study). Greater shrinkage due to histological processing of the tissue, as well as the less exact orientation (inclination of the central cochlea axis) before imaging with plastic casts might explain these differences. Furthermore, the localization of the center of the RW, the central axis of the cochlea, and the connection point of the opposing wall could cause deviations in the clinical CT images or plastic casts. Although the differences are not generally large, it is very likely that the present method was less susceptible to these methodological biases. Comparison of the standard deviations clearly indicates that μCT allowed higher precision measurements than was the case in previous investigations.

We found a statistically significant correlation between the LCB and the WCB ($R^2 = 0.71$), which was higher than in Escude et al. (2006) ($R^2 = 0.57$). The difference may be explained by the more precise virtual reorienting in the present study compared with the previous study. Furthermore, we observed that the length and width of the cochlear base were also linearly proportional to the length along the lateral wall of the ST. In contrast, we were unable to find any correlation between the cochlear axis height and any dimension of the basic measurements, which again is in accordance with Dimopoulos and Muren (1990).

In addition, we found a correlation between spiral ganglion length and the distance along the lateral wall of the ST ($R^2 = 0.83$). Stakhovskaya et al. (2007) found a corresponding correlation between the length of the spiral ganglia and that of the organ of Corti ($R^2 = 0.76$). The correlations between the distance along the ST, size of the cochlea, and length of the spiral ganglion provide a good method to define the required insertion depth of a CI electrode array in a particular patient based on preoperative imaging.

Advanced measurements of scala tympani height

Previous reports on the central height of the ST (Hatsushika et al., 1990; Igarashi et al., 1976; Merzenich et al., 1979; Walby, 1985; Wysocki, 1999; Zrunek and Lischka, 1981; Zrunek et al., 1980; Zwislocki, 1948) showed a discontinuous decrease from base to apex. We measured the height at the modiolar, central, and lateral locations instead of determining the maximum height. This approach allowed us to relate the measure obtained to the modiolar–antimodiolar position, providing additional information of particular interest for cochlear prostheses. Our heights discontinuously decreased with increasing distance from RW at the central and lateral position of the scala, whereas the height at the modiolar position remained nearly constant. Due to flattening of the ST shape at around the 450° position, the height decreased toward the lateral wall. The crucial decrease in lateral height beyond 450° likely increases the risk of unwanted contact between the upper part of the electrode and the basilar membrane, the spiral ligament, or the osseous spiral lamina, which can lead to intracochlear trauma. Walby (1985) showed that the height of the ST at the center of the ST decreased in the first 9 mm distance from the RW. This region corresponds to 140° and accords well with our data. The central height showed a slight increase between 22 and 23 mm (410–460°) from the RW in the present study, which is again in agreement with previous data: Zwislocki (1948) measured a slight increase between 20 and 27 mm, whereas Zrunek and Lischka (1981) measured an increase of around 21–22 mm, and Merzenich et al. (1979) between 14 and 22 mm from the RW.

The ST has an initial oval shape at the beginning of the RW, with the long axis in the vertical direction. This initial shape changes to an oval shape, with the long axis in the horizontal direction, resulting in greater heights within the first 30° (2–3 mm from the RW). The plateau between the 150 and 400° positions (10–21 mm) is in line with the findings of Wysocki (1999), and those of Zrunek and Lischka (1981). Our height values

were slightly larger than those in previous studies. This is most likely attributable to the more precise measurement method in the present study. Furthermore, the irregular cross sections of the casts may distort the real size of the intracochlear dimensions of the ST.

Cross-sectional diameter and sectional area

Because of the rounded shape of CI electrode arrays and the limited size of the ST, a circular fit allows an estimation of the dimensional limitations for the electrode array, whereby the sectional area shows the maximum available space in the ST. Comparison of the aCSD and the aSA showed that the CSD fills an average 82% of the SA (range: 55–95%). The measurements of the SA are in line with those of Zrunek and Lischka (1981), who measured the sectional areas from molded cochleae. The comparison of the average cross-sectional diameter and the mean central height (plot not included) showed that they are similar up to 18 mm from the RW. From that point, the aCSD shifts more toward the modiolar wall and becomes smaller than the mean central height. The progression of the CSD curve in the present study is in accordance with Biedron et al. (2010), who measured the diameter manually. In addition to the interindividual variability of the CSD, the overall pattern and the position of the CSD minima and maxima also exhibited interindividual variations. The aCSD showed two considerable reduction of the ST: between 60 and 180°, where the aCSD decreased by 0.25 mm, and beyond the 450° position. At those two points, insertion trauma was frequently reported (Aschendorff et al., 2003; Eshraghi et al., 2003; Nadol et al., 2001; Richter et al., 2001; Tykocinski et al., 2001; Wardrop et al., 2005b). This can be related to the present finding with regard to CSD, combined with the vertical trajectory that results either in peaks in some cochleae, or in an increase in vertical position following a previous dip, thus orienting the implant against the basilar membrane.

Cochlear length measures: angle versus distance measures

Owing to the variability of the ST length, the angular position for a CI electrode array will be different from subject to subject. We measured the distance along the center and along the lateral wall of the ST starting from the anterior/inferior edge of the RW and described the relationship to the angular distance. The variation in cochlear length (centrally and laterally) between the scalae increased as it was measured further away from the RW toward the end of the second turn due to the continuous tighter coiling of the cochlea.

The length along the lateral wall showed slightly larger variation than did the length along the center of the scala. Stakhovskaya et al. (2007) found the same trend for the distance along the spiral ganglion, and also for the distance along the organ of Corti.

Our measurements along the lateral wall (mean distance for 360°: 21 mm, range: 18.5–23 mm) yielded slightly lower values than those obtained in previous studies (Erixon et al., 2008; Erixon and Rask-Andersen, 2013; Kawano et al., 1996; Stakhovskaya et al., 2007). The likeliest explanation is that the exact point of measurement was different. We determined the distance at the most lateral point inside the ST, whereas Erixon and Rask-Andersen (2013) did so along the outer wall of the cochlea (mean distance for 360°: 22.8 mm; range: 20.7–24.2 mm). Stakhovskaya et al. (2007) and Kawano et al. (1996) measured the distance along the organ of Corti and reported a mean distance for 360° between 20.5 and 20.9 mm, which is closer to our mean value for 360°.

Stakhovskaya et al. (2007) suggested an equation to predict the percentage of the length of the organ of Corti for a desired angular distance. Erixon and Rask-Andersen (2013) predicted a formula to estimate the basal and two-turn length for a given length of the cochlear base. Equation (2) (proposed above) additionally allows prediction of the insertion distance laterally and at the center of the ST for a desired angular distance. Even though this equation already provides a good estimate of individual cochlear length, the interindividual variability in angle–distance relations indicates that the differences in cochlear size are due to partially disproportional growth of the cochlea with regard to macroscopic dimensions.

Vertical trajectory and cochlear damage during implantation

The basic and advanced measurements give detailed information on cochlear dimensions, with the ST's vertical trajectory providing detailed information on some of its morphological variations. Based on the vertical trajectory, we divided the scalae into three different categories. Three critical anatomic features were identified with an increased risk of cochlear trauma during insertion of CI electrode array: dips, peaks, and vertical jumps.

The scalae in the rollercoaster category were different from other scalae due to their initial downward-oriented trajectory, with a distinct local minimum (dip). For these scalae, a correct insertion angle for a CI

electrode array is critical to avoid basilar membrane damage in the very first portion of the cochlea, where the implant might come into contact with the basilar membrane around the dip position. Furthermore, cochleostomies in such cases should not be placed too far anteriorly from the RW. Correspondingly, Huettenbring et al. (2002) and O'Leary et al. (1991) reported some insertion trauma at the base of the basal turn. Another critical point is around 180°, at which point the implant in these cochleae would first be oriented downward, and then upward to reach the antimodiolar wall at the point where the cochlea turns to the side. This might push the implant against the basilar membrane.

Moreover, in both the rollercoaster and intermediate categories, vertical jumps were located between the 450 and 500° positions. This is the point at which the first and second turns of the cochlea are close to each other and where the ST appears to be deflected upward. These sudden jumps may result in the electrode array tip getting stuck at that location, and may lead to buckling of the electrode array or deviation from the ST trajectory and displacement toward the scala vestibuli.

The scalae in the sloping category had peaks around 180° from the RW. If the electrode array does not continue to closely follow the vertical trajectory of the scala beyond that point, it will rupture the basilar membrane. The risk of electrode dislocation is especially high at this point due to the electrode array making contact with the lateral wall. It might follow a movement in the vertical direction instead of a lateral one. A flattening of the ST was typically observed at this point as well. This condition is likely to result in cochlear damage during implantation (Helbig et al., 2011; Kha and Chen, 2012; Nadol et al., 2001; Richter et al., 2001; Tykocinski et al., 2001; Wardrop et al., 2005a), with rupturing of the basilar membrane at the location about 10–15 mm along the lateral wall of the ST from the RW. Slow insertion of the electrode array might minimize insertion trauma at 180°. When the point of first resistance is reached at that location, reinsertion of the electrode array is potentially an option. The two scalae of the intermediate group had a similar vertical trajectory here. They showed vertical jumps between 15 and 18 mm, but, unlike scalae in the other two categories, they did not exhibit dips or peaks.

To overcome the vertical jump between 15 and 18 mm, adjusted insertion speed would minimize insertion trauma. Furthermore, deep insertion in rollercoaster cochleae is likely to result in cochlear damage, either at the 180° region or at the region where the second turn begins. Finally, midmodiolar and perimodiolar locations of the implant are likely to result in less damage, owing to the availability of more intrascalar space to accommodate the electrode array.

The location of dips, peaks, and vertical jumps correlated with the findings of Verbist et al. (2009), who found the majority of dips and vertical jumps around 45, 90, 270, and 450°, whereas peaks were concentrated around 180 and 675°. The criteria used to define anatomical features were, however, stricter in the present study.

CONCLUSIONS

μCT allowed highly precise measurements of human cochlear dimensions. The large anatomic variability between different cochleae has considerable implications for the design of CI electrode arrays, especially with respect to their atraumaticity. The flattening and the possible presence of dips, peaks, and vertical jumps are one important reason for dislocation of cochlear implant electrode arrays into the scala media and scala vestibuli, and the consequent damage to basilar membrane and surrounding tissue. Our data demonstrate the need for an individualized cochlear implant electrode array and an adjusted insertion procedure taking into account the individual cochlear length and, ideally, the microanatomy as well. Cochlear base measurements can be used to determine the required lengths for both lateral and midscalar locations of the implant. Further studies will investigate the correlation among preoperative CT scans (length and width of the cochlear base), the cross-sectional diameter of the scala tympani, and the possibility of differentiating between the sloping and rollercoaster cochlear configuration.

ACKNOWLEDGMENTS

The authors thank Drs. Tim Holden and Jill Firszt at Washington University School of Medicine, St. Louis, MO for providing five μCTs in support of this study.

CONFLICT OF INTEREST STATEMENT

The authors have no conflicts of interest, including any financial, personal, or other relationships with other people or organizations known or identified.

ROLE OF AUTHORS

All authors had full access to all the data in the study and take responsibility for the integrity of the data and the accuracy of the data analysis. Study concept and design: TN, VH, AK; Acquisition of data: EA, TN; Analysis of data: EA, TN; Interpretation of the data: EA, TN, TL, VH, AK; Drafting of the manuscript: EA, TN, AK; Critical revision of the manuscript for important

intellectual content: VH, TL, AK; Statistical analysis: EA; Obtained funding: VH, AK; Administrative, technical, and material support: EA, TN; Study supervision: VH, AK.

LITERATURE CITED

Adunka O, Kiefer J. 2006. Impact of electrode insertion depth on intracochlear trauma. Otolaryngol Head Neck Surg 135:374–382.

Aschendorff A, Klenzner T, Richter B, Kubalek R, Nagursky H, Laszig R. 2003. Evaluation of the hifocus electrode array with positioner in human temporal bones. J Laryngol Otol 117:527–531.

Biedron S, Prescher A, Ilgner J, Westhofen M. 2010. The internal dimensions of the cochlear scalae with special reference to cochlear electrode insertion trauma. Otol Neurotol 31:731–737.

Cullen RD, Higgins C, Buss E, Clark M, Pillsbury HC, Buchman CA. 2004. Cochlear implantation in patient with substantial residual hearing. Laryngoscope 114:2218–2223.

Dimopoulos P, Muren C. 1990. Anatomic variations of the cochlea and relation to other temporal bone structures. Acta Radiol 31:439–444.

Erixon E, Rask-Andersen H. 2013. How to predict cochlear length before cochlear implantation surgery. Acta Otolaryngol 133:1258–1265.

Erixon E, Hoegstorp H, Wadin K, Rask-Andersen H. 2008. Variational anatomy of the human cochlea: implications for cochlear implantation. Otol Neurotol 30:14–22.

Escude B, James C, Deguine O, Cochard N, Eter E, Fraysse B. 2006. The size of the cochlea and predictions of insertion depth angles for cochlear implant electrodes. Audiol Neurotol 11:27–33.

Eshraghi AA, Yang NW, Balkany TJ. 2003. Comparative study of cochlear damage with three perimodiolar electrode designs. Laryngoscope 113:415–419.

Gantz BJ, Turner CW. 2003. Combining acoustic and electric hearing. Laryngoscope 1113:1726–1730.

Hardy M. 1938. The length of the organ of Corti in man. Am J Anat 62:291–311.

Hatsushika S, Shepherd RK, Tong YC, Clark GM, Funasaka S. 1990. Dimensions of the scala tympani in the human and cat with references to cochlear implants. Ann Otol Rhinol Laryngol 99:871–876.

Helbig S, Settevendemie C, Mack M, Baumann U, Helbig M, Stoever T. 2011. Evaluation of an electrode prototype for atraumatic cochlear implantation in hearing preservation candidates: preliminary results from a temporal bone study. Otol Neurotol 32:342–360.

Holden LK, Finley CC, Firszt JB, Holden TA, Brenner C, Potts LG, Gotter BD, Vanderhoof SS, Mispagel K, Heydebrand G, Skinner MW. 2013. Factors affection open-set word recognition in adults with cochlear implants. Ear Hear 34:342–360.

Huettenbring KB, Zhanert T, Jolly C, Hofmann G. 2002. Movements of cochlear implant electrodes inside the cochlea during insertion: an x-ray microscopy study. Otol Neurotol 23:187–191.

Igarashi M, Takahashi M, Alford BR. 1976. Cross-sectional area of scala tympani in human and cat. Arch Otolaryngol 102:428–429.

Kawano A, Seldon HL, Clark GM. 1996. Computer-aided three-dimensional reconstruction in human cochlear maps: measurement of the length of organ of Corti, outer wall, inner wall, and Rosenthal's canal. Ann Otol Rhinol Laryngol 105:701–709.

Kha H, Chen B. 2012. Finite element analysis of damage by cochlear implant electrode arrays proximal section to the basilar membrane. Otol Neurotol 33:1176–1180.

Kral A, O'Donoghue GM. 2010. Profound deafness in childhood. N Engl J Med 363:1438–1450.

Leake PA, Hradek GT, Snyder RL. 1999. Chronic electrical stimulation by a cochlear implant promotes survival of spiral ganglion neurons after neonatal deafness. J Comp Neurol 412:543–562.

Lenarz T. 1998. Cochlear implants: selection criteria and shifting borders. Acta Otorhinolaryngol Belg 52:183–199.

Lenarz T. 1999. Sensorineural hearing loss in children. Int J Pediatr Otorhinolaryngol 49:179–181.

Lenarz T, editor. 2009. Electro-acoustic stimulation of the cochlea: 2nd International Electro-Acoustic Workshop, Hannover, 2007. Audiol Neurotol 14(suppl1).

Martinez-Monedero R, Niparko JK, Aygun N. 2011. Cochlear coiling pattern and orientation differences in cochlear implant candidates. Otol Neurotol 32:1086–1093.

Merzenich MM, Byers CL, Walsh SM. 1979. Development of multichannel electrodes for an auditory prosthesis. 9th quarterly progress report of NIH. Bethesda, MD, National Institutes of Health.

Miller JD. 2007. Sex differences in the length of the organ of Corti in humans. J Acoust Soc Am 121:151–155.

Min KS, Jun SB, Lim YS, Park SI, Kim SJ. 2013. Modiolus-hugging intracochlear electrode array with shape memory alloy. Comput Math Methods Med 2013:1–9.

Nadol JB, Burgess B, Gantz BJ, Coker NJ, Ketten DR, Kos I, Roland JT, Shiao JY, Eddington DK, Montandon P, Shallop JK. 2001. Histophatology of cochlear implants in humans. Ann Otol Rhinol Laryngol 110:883–891.

O'Leary MJ, Fayad J, House WF, Linthicum FH. 1991. Electrode insertion trauma in cochlear implantation. Ann Otol Rhinol Laryngol 100:695–699.

Postnov A, Zarawski A, De Clerck N, Vanpoucke F, Offeciers FE, Van Dyck D, Peeters S. 2006. High resolution micro-CT scanning as an innovative tool for evaluation of the surgical positioning of cochlear implant electrodes. Acta Otolaryngol 126:467–474.

Rask-Andersen H, Erixon E, Kinnefors A, Loewenheim H, Schrott-Fischer A, Liu W. 2011. Anatomy of the human cochlea: implications for cochlear implantation. Cochlear Implants Int 12:S8–13.

Ravicz ME, Merchant SN, Rosowski JJ. 2000. Effect of freezing and thawing on stapes-cochlear input impedance in human temporal bones. Hear Res 150:215–224.

Rebscher SJ, Hetherington A, Bonham B, Wardrop P, Whinney D, Leake PA. 2008. Considerations for design of future cochlear implant electrode arrays: electrode array stiffness, size, and depth of insertion. J Rehabil Res Dev 45: 731–748.

Richter B, Aschendorf A, Lohnstein P, Husstedt H, Nagursky H, Laszig R. 2001. The nucleus contour electrode array: a radiological and histological study. Laryngoscope 111: 508–514.

Roland PS, Wright CG. 2006. Surgical aspects of cochlear implantation: mechanisms of insertional trauma. Adv Otorhinolaryngol 64:11–30.

Rosowski JJ, Davis PJ, Merchant SN, Donahue KM, Coltrera MD. 1990. Cadaver middle ears as models for living ears: comparisons of middle ear input immittance. Ann Otol Rhinol Laryngol 99:403–412.

Shin KJ, Lee JY, Kim JN, Yoo JY, Shin C, Song WC, Koh KS. 2013. Quantitative analysis of the cochlea using three-dimensional reconstruction based on microcomputed tomographic images. Anat Rec 296:1083–1088.

Simmons FB. 1967. Permanent intracochlear electrodes in cats, tissue tolerance and cochlear microphonics. Laryngoscope 77:171–186.

Skinner MW, Ketten DR, Holden LK, Harding GW, Smith PG, Gates GA, Neely JG, Kletzker GR, Brunsden B, Blocker B. 2002. CT-derived estimation of cochlear morphology and electrode array position in relation to word recognition in Nucleus-22 recipients. J Assoc Res Otolaryngol 3:332–350.

Staecker H, Gabaizadeh R, Federoff H, Van de Water TR. 1998. Brain-derived neurotrophic factor gene therapy prevents spiral ganglion degeneration after hair cell loss. Otolaryngol Head Neck Surg 119:7–13.

Stakhovskaya O, Shridhar D, Bonham BH, Leake PA. 2007. Frequency map for the human cochlear spiral ganglion: implications for cochlear implants. J Assoc Res Otolaryngol 8:220–233.

Turner CW, Gantz BJ, Vidal C, Behrens A, Henry BA. 2004. Speech recognition in noise for cochlear implant listeners: benefits of residual acoustic hearing. J Acoust Soc Am 115:1729–1735.

Tykocinski M, Saunders E, Cohen LT, Treaba C, Briggs RJ, Gibson P, Clark GM, Cowan RS. 2001. The contour electrode array: safety study and initial patient trials of a new perimodiolar design. Otol Neurotol 22:33–41.

Verbist BM, Ferrarini L, Briaire JJ, Zarowski A, Admiraal-Behloul F, Olofsen H, Reiber JH, Friins JH. 2009. Anatomic considerations of cochlear morphology and its implications for insertion trauma in cochlear implant surgery. Otol Neurotol 30:471–477.

Verbist BM, Skinner MW, Cohen LT, Leake PA, James C, Boex C, Holden TA, Finley CC, Roland PS, Roland JT, Haller M, Patrick JF, Jolly CN, Faltys MA, Briaire JJ, Friins JH. 2010. Consensus panel on a cochlear coordinate system applicable in histologic, physiologic, and radiologic studies of the human cochlea. Otol Neurotol 31:722–730.

Von Illberg C, Kiefer J, Tillein J, Pfenningdorff T, Hartmann R, Stuerzbecher E, Klinke R. 1999. Electric-acoustic stimulation of the auditory system. New technology for severe hearing loss. ORL J Otorhinolaryngol Relat Spec 61:334–340.

Walby AP. 1985. Scala tympani measurement. Ann Otol Rhinol Laryngol 94:393–397.

Wardrop P, Whinney D, Rebscher SJ, Luxford W, Leake PA. 2005a. A temporal bone study of insertion trauma and intracochlear position of cochlear implant electrodes. II: Comparison of Spiral Clarion and HiFocus II electrodes. Hear Res 203:68–79.

Wardrop P, Whinney D, Rebscher SJ, Roland JT, Luxford W, Leake PA. 2005b. A temporal bone study of insertion trauma and intracochlear position of cochlear implant electrodes. I: Comparison of Nucleus banded and Nucleus Contour electrodes. Hear Res 203:54–67.

Wysocki J. 1999. Dimensions of the human vestibular and tympanic scalae. Hear Res 135:39–46.

Zrunek M, Lischka M. 1981. Dimensions of the scala vestibuli and sectional areas of both scales. Arch Otorhinolaryngol 233:99–104.

Zrunek M, Lischka M, Hochmair-Desoyer I, Burian K. 1980. Dimensions of the scala tympani in relation to the diameters of multichannel electrodes. Arch Otorhinolaryngol 229:159–165.

Zwislocki M. 1948. Theorie der Schneckenmechanik. Acta Otolaryngol 72:1–71.